U-J synergy effect for high-T_c superconductors

Liliana Arrachea[1,2,*] and Dražen Zanchi[2]
[1]*Departamento de Física, Universidad de Buenos Aires, Ciudad Universitaria Pabellón I, (1428) Buenos Aires, Argentina*
[2]*Laboratoire de Physique Théorique et Hautes Énergies, 4 Place Jussieu, 75252 Paris Cedex 05, France*
(Received 7 September 2004; published 28 February 2005)

Using the renormalization group with included self-energy effects and exact diagonalization of small clusters we investigate the ground-state phase diagram of a two-dimensional extended Hubbard model with nearest-neighbor exchange interaction J, in addition to the local Coulomb repulsion U. The main instabilities are antiferromagnetism close to half filling and $d_{x^2-y^2}$ superconductivity in the doped system. We find that self-energy effects are fatal for superconductivity in the repulsive Hubbard model (i.e., $J=0$, $U>0$). The superconductivity is *triggered* by finite J. The combined action of J and U interactions provide a remarkably efficient, mechanism to enhance both $d_{x^2-y^2}$ superconducting and antiferromagnetic correlations.

DOI: 10.1103/PhysRevB.71.064519 PACS number(s): 74.20.Mn, 71.10.Fd

I. INTRODUCTION

One of the most striking features observed in the phase diagram of the high-T_c superconducting cuprates is the proximity between the insulating state with long-range antiferromagnetic order and the superconducting phase. This remarkable issue and the fact that at optimum doping the antiferromagnetic coherence length remains finite ($\xi \sim 4a$ for $La_{2-x}Sr_xCu0_4$), have been the source of inspiration for many theoretical works in which the pairing mechanism is proposed to be originated in the fluctuations of the spin-density wave phase. Another peculiarity of these materials is that the superconducting order parameter has $d_{x^2-y^2}$ symmetry. The reason for this property is also thought to be the closeness to the antiferromagnetic phase as the lines of nodes of the superconducting gap allows for the existence of gapless spin excitations and superconductivity can coexist with spin-density wave fluctuations. Very recently, the proximity between these two phases supplemented with the effect of disorder has been the basic ingredient in a phenomenological model to suggest that *colossal* effects can be expected in the phase diagram of the cuprates.[1]

The fact that the ground state of the undoped materials is antiferromagnetic immediately suggests that the Hubbard model could be a good candidate for a microscopic description of these compounds. Instead, the explanation of the superconducting mechanism in the framework of this model remains very controversial. A superconducting solution is found when the model is tackled with some many-body techniques.[2–10] However, all the numerical works devoted to search indications of superconductivity in the repulsive Hubbard model have been negative so far.[11–14] Another candidate model to provide the basis for the theoretical investigation of the high-T_c superconductors is the *t-J* model, which coincides with the Hubbard Hamiltonian in the limit of $U \to \infty$ (corresponding to $J \to 0$). In the case of the *t-J* model, many-body methods and numerical results seem to be in agreement concerning the possibility of a superconducting state with $d_{x^2-y^2}$ symmetry.[15–18] The range of J at which it may occur is, however, not precisely determined and it is likely to lie beyond the region where the mapping from the Hubbard model is valid.

This motivates the study of the *t-J-U* model

$$H = -t\sum_{\langle ij\rangle,\sigma}(c^{\dagger}_{i\sigma}c_{j\sigma} + \text{H.c.}) + J\sum_{\langle ij\rangle}\mathbf{S}_i\cdot\mathbf{S}_j + U\sum_i n_{i\uparrow}n_{i\downarrow}, \quad (1)$$

which, in addition to the Coulomb repulsion U of the usual Hubbard Hamiltonian, contains a nearest-neighbor exchange interaction J as the *t-J* model. In such a way, we can expect to retain appealing features of both models, like the charge fluctuations introduced by U but forbidden in the constrained *t-J* model and the robust superconducting correlations introduced by the exchange interaction and explore the interplay between both effects. In addition to these heuristic arguments, the *t-J-U* model is closely related to the extended Hubbard model with correlated hopping, which has been derived from the three-band extended Hubbard model as an effective one-band Hamiltonian to describe the low energy properties of the Cu-O planes of the high-T_c materials.[19] The latter model is characterized by three different nearest-neighbor hopping amplitudes t_{AA}, t_{AB}, t_{BB} depending on the occupation of the two sites involved, as well as the usual Coulomb repulsion U,

$$H = U\sum_i n_{i\uparrow}n_{i\downarrow} - \sum_{\langle ij\rangle,\sigma}(c^{\dagger}_{i\sigma}c_{j\sigma} + \text{H.c.})\{t_{AA}(1-n_{i\bar{\sigma}}) \times (1-n_{j\bar{\sigma}})t_{AB}[(1-n_{i\bar{\sigma}})n_{j\bar{\sigma}}) + n_{i\bar{\sigma}}(1-n_{j\bar{\sigma}})]t_{BB}n_{i\bar{\sigma}}n_{j\bar{\sigma}}. \quad (2)$$

Each of the parameters of the above model depend on the parameters of the original three-band Hamiltonian and there is a degree of uncertainty in their precise values. The relevant property is that reasonable estimates indicate that t_{AB} is larger than the other two.[19] The analysis of the different hopping processes in Eq. (2) reveals that the one driven by t_{AB} mediates antiferromagnetic correlations. In particular, in the strong coupling limit $U \gg t_{AA}, t_{AB}, t_{BB}$, the exchange interaction obtained by treating Eq. (2) with second order perturbation theory is $J = 4t^2_{AB}/U$. Furthermore, when this process is suppressed, antiferromagnetic correlations are completely eliminated and a metal-insulator transition can take place at finite U in the half-filled system.[20–22] For weak coupling, the

Hamiltonian (2) can be treated with mean-field Hartree-Fock and BCS-like techniques in two dimensions (2D) (Ref. 23) and with operator product expansion and bosonization in 1D.[24] It turns out that, close to half filling, the predicted phase diagram is equivalent to that obtained starting from an effective *t-J-U* model.[25] In summary, the relevance of the *t-J-U* model to describe the physics of the cuprates can be also supported by its closeness to the correlated Hubbard model derived from the more detailed three-band Hubbard model for the Cu-O planes.

Coming back to the phenomenology of the superconducting cuprates, the *t-J-U* model provides the framework for recent suggestions based on a combined order parameter with superconducting and bond-density-wave components with $d_{x^2-y^2}$ symmetries to explain the intriguing pseudogap phenomena.[26] In general, extended Hubbard models in low dimensions are of interest in the context of high-T_c materials[27–29] and also to understand the rich structure observed in the phase diagrams of organic materials such as $(TMTSF)_2PF_6$ and $(TMTSF)_2ClO_4$,[22,24,30–37] which cannot be explained on the basis of the local Coulomb interaction of the usual Hubbard model.

The *t-J-U* model has an explicit effective attraction mediated by *J* that enables a superconducting solution even within a simple BCS-like description. Numerical studies of this model in ladders indicate that superconducting correlations with $d_{x^2-y^2}$ symmetry are enhanced in comparison to those of the usual Hubbard model.[38] More recently, an analysis based on the Landau-Fermi-liquid picture has been adopted to argue that the pairing interaction mediated by *J* combined by a strong renormalization of the effective density of states caused by *U* results in a significant enhancement of the superconducting order parameter while quantum Monte Carlo simulations based on a variational wave function with a BCS structure support this picture.[39] Investigations of the weak coupling phase diagram at van Hove fillings of the two-dimensional version of this model supplemented by a nearest-neighbor Coulomb repulsion and next-nearest-neighbor hopping amplitude have also been reported.[40]

The aim of this work is to investigate the two-dimensional phase diagram of the *t-J-U* model with two complementary techniques: exact diagonalization (ED) of a small cluster with 4×4 sites and the one-loop renormalization group (RG) technique presented in Refs. 6, 41. The latter are expected to provide reliable indications of the main instabilities of the Fermi liquid in the limit of weak interactions. ED is an unbiased method that consists in the exact calculation of the ground-state wave function, allowing for the direct evaluation of the relevant correlation functions but has the drawback that the size of the clusters that are amenable to be treated is small. In spite of that limitation, in the case of the *t-J* model, the conclusions based on numerical results on such small clusters are among the most robust ones regarding superconductivity.[17] It is therefore interesting to analyze the predictions of these two methods and to compare them with previous results.

The article is organized as follows, in Sec. II we provide some technical details on the methods we employ. In particular, we describe the procedure followed to include self-energy corrections in the RG treatment. An important reference is the behavior of the relevant susceptibilities evaluated with this RG procedure for the usual Hubbard model. This is discussed in Sec. III. In Sects. IV and V we present the results for the *t-J-U* model using RG and ED, respectively. Section VI is devoted to summary and conclusions.

II. TECHNICAL DETAILS

A. Renormalization group method

The basic hypothesis of the renormalization group method is that the normal state is well described by the effective action for quasiparticles near the Fermi surface. The description of the many body problem is done in terms of the two-body effective interaction $U_l(\theta_1,\theta_2,\theta_3)$ and the quasiparticle weight $Z_l(\theta)$. In the Wilson's renormalization scheme, $U_l(\theta_1,\theta_2,\theta_3)$ is the effective interaction between electrons *within* the ring $\pm\Lambda$ around the Fermi surface. This interaction is renormalized by the scattering processes involving all electrons *outside* the ring $\pm\Lambda$. A physical interpretation of the cutoff Λ is that it plays the role of an effective temperature or the experimental probe frequency. In previous versions of RG,[6,8,9,40] it was assumed $Z_l(\theta)=1$. In what follows, we summarize the improved RG method of Ref. 41 which also considers self-energy corrections by taking into account the renormalization of the quasiparticle weight.

An important issue to note is the fact that $U_l(\theta_1,\theta_2,\theta_3)$ and $Z_l(\theta)$ depend only on the angles θ_i that parametrize the positions of the particles on the Fermi surface. This is justified by a simple power counting which tells us that only the angular dependence of the effective interaction is marginal (or marginally relevant) and only terms up to linear in energy are to be kept in the renormalization of the angle-dependent self-energy.[41] In the renormalization group procedure, these functions are continuously renormalized as the energy cutoff, parametrized by the scale l as $\Lambda=8t\exp(-l)$ is reduced. The ensuing equation for the evolution of U_l within the one-loop renormalization group scheme has the following structure:

$$\frac{\partial U_l}{\partial_l}=\beta_{pp}\{U_l,U_l\}+2\beta_{ph}\{U_l,U_l\}-\beta_{ph}\{U_l,XU_l\}-\beta_{ph}\{XU_l,U_l\}-X\beta_{ph}\{XU_l,XU_l\}, \tag{3}$$

where X is the exchange operator defined as $XU(1,2,3)=U(2,1,3)$. One must remember that Eq. (3) is a *functional* flow equation, i.e., U_l and all terms on the right-hand side depend on three angles $(\theta_1,\theta_2,\theta_3)$. Particle-particle (Cooper) and particle-hole (density-wave) differential bubbles β_{pp} and β_{ph} are shown on Fig. 1.

To solve numerically Eq. (3) we discretize the angle θ which defines the so-called *N*-patch model. The function $U_l(\theta_1,\theta_2,\theta_3)$ is then represented by a set of coupling constants labeled by three discrete indexes. For the *t-J-U* model, the initial condition is

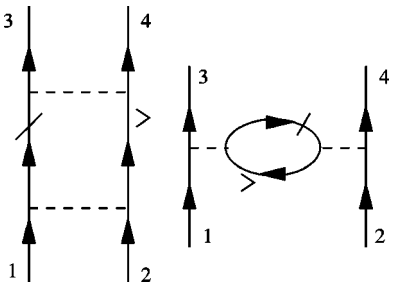

FIG. 1. Propagators corresponding to degrees of freedom on the shell $\pm\Lambda$ are indicated with a bar, while propagators of degrees of freedom outside the ring $\pm\Lambda$ are denoted with an arrow.

$$U_{l=0}(\theta_1,\theta_2,\theta_3)=\left\{U-\frac{J}{4}[\cos(x_3-x_1)+\cos(y_3-y_1)]-\frac{J}{2}[\cos(x_3-x_2)+\cos(y_3-y_2)]\right\}, \quad (4)$$

where (x_i,y_i) are components of the wave vector $\mathbf{k}_i$, corresponding to the angle θ_i at the noninteracting Fermi surface. All coupling constants are found to diverge at the same critical scale l_c as

$$U_l(\theta_1,\theta_2,\theta_3)\to\frac{\tilde{U}(\theta_1,\theta_2,\theta_3)}{l_c-l}, \quad (5)$$

where the weights $\tilde{U}$ are model dependent constants. This type of solution is called the fixed-pole solution in contrast to the mobile-pole solution, where different coupling constants diverge at different critical scales. For realistic systems, where the initial coupling is not extremely small, only fixed poles are relevant.[42] The critical scale l_c depends on the bare coupling constants U and J and on the band filling parametrized by the chemical potential. The critical cutoff $\Lambda_c=8t\exp(-l_c)$ appears to be the characteristic temperature of the model. The most precise nonrestrictive interpretation of Λ_c is that at this energy electrons start to build bound states. Namely, the poles in Eq. (5) are the two-particle propagator poles, indicating the onset of bound states. These bound states can be of charge, spin or superconducting kind and all of them renormalize the one-particle weight. This renormalization is angle dependent and its evolution is described by the following expression:

$$\partial_l \ln Z_l(\theta)=\frac{1}{(2\pi)^2}\int d\theta' \mathcal{I}(\theta',-\Lambda)\eta_l(\theta,\theta'), \quad (6)$$

with the initial condition $Z_l(\theta)=1$. The function $\mathcal{I}(\theta,\epsilon)$ is the angle-dependent density of states at the energy ϵ (measured from the Fermi level). The quantity $\eta_l(\theta,\theta')$ contains particle-particle (*pp*) and particle-hole (*ph*) contributions

$$\eta_l(\theta,\theta')\equiv(2X-1)\beta_{pp}\{U_l,U_l\}+2\beta_{ph}\{XU_l,XU_l\}+2\beta_{ph}\{U_l,U_l\}-\beta_{ph}\{U_l,XU_l\}-\beta_{ph}\{XU_l,U_l\} \quad (7)$$

with all terms on the right-hand side taken with external legs $(\theta_1,\theta_2,\theta_3)=(\theta,\theta',\theta')$. The interaction inserted in all beta functions obeys the scaling Eq. (3). The relation between interaction U_l and the usual physical interaction Γ contains the rescaling Z factors[41]

$$\Gamma_l(1,2,3)=[Z_l(1)Z_l(2)Z_l(3)Z_l(4)]^{-1/2}U_l(1,2,3). \quad (8)$$

To find out which correlations are relevant and candidates for order parameter we must allow the theory to choose between all possible two-particle correlations. For this reason we have to follow the renormalization of several angle-resolved correlation functions. The superconducting correlation function $\chi_l^{\mathrm{SC}}(\theta_1,\theta_2)$ measures correlations between the Cooper pairs $(\theta_1,\theta_1+\pi)$ and $(\theta_2,\theta_2+\pi)$, all states being at the Fermi surface. The antiferromagnetic correlation function $\chi_l^{\mathrm{AF}}(\theta_1,\theta_2)$ correlates two nested electron-hole pairs $c^\dagger_{\mathbf{k}(\theta_1)}\sigma c_{\mathbf{k}(\theta_1)+(\pi,\pi)}$ and $c^\dagger_{\mathbf{k}(\theta_2)}\sigma c_{\mathbf{k}(\theta_2)+(\pi,\pi)}$. The charge density wave correlation function $\chi_l^{\mathrm{CDW}}(\theta_1,\theta_2)$ correlates the nested chargelike electron-hole pairs. To get the renormalization group flow of all correlation functions we follow the procedure given in Ref. 6 but dressing the electronic propagators with Z factors as in Ref. 41. We get

$$\chi_l^\delta(\theta_1,\theta_2)=\frac{1}{Z_l(\theta_1)Z_l(\theta_2)}\oint d\theta\, \tilde{z}_l^\delta(\theta_1,\theta)D_l^\delta(\theta)\tilde{z}_l^\delta(\theta,\theta_2). \quad (9)$$

The function $D_l^\delta(\theta)$ is written

$$D_l^{\mathrm{SC}}(\theta)=\frac{1}{2}\sum_{\nu=+,-}\mathcal{I}[\nu\Lambda(l),\theta] \quad (10)$$

for the SC channel and

$$D_l^{\mathrm{AF}}(\theta)=\frac{1}{2}\frac{\mathcal{I}[-\Lambda(l),\theta]}{1+|\mu|/\Lambda(l)}, \quad (11)$$

for the AF channel where only the negative shell ($\nu=-1$) contributes to the flow.

The flow of the quantity $\tilde{z}_l^\delta(\theta_1,\theta)$ that has the role of a triangular vertex is written

$$[\partial_l-\eta(\theta_1)-\eta(\theta_2)]\tilde{z}_l^\delta(\theta_1,\theta_2)=-\oint d\theta\,\tilde{z}_l^\delta(\theta_1,\theta)D_l^\delta(\theta)V_l^\delta(\theta,\theta_2). \quad (12)$$

The meaning of $\tilde{z}_l^\delta(\theta_1,\theta_2)$ is that

$$\tilde{z}_l^\delta(\theta_1,\theta_2)\equiv Z_l(\theta_1)z_l^\delta(\theta_1,\theta_2)Z_l(\theta_2)$$

so that the initial conditions for $\tilde{z}_l^\delta$ and for z_l^δ are the same:

$$z_{l=0}^\delta(\theta_1,\theta_2)=\delta_D(\theta_1-\theta_2), \quad (13)$$

where δ_D is the Dirac function. Initial conditions for susceptibilities are

$$\chi_{l=0}^\delta(\theta_1,\theta_2)=0. \quad (14)$$

After discretization we integrate numerically Eqs. (9) and (12). The relevant susceptibility in each channel is the dominant eigenvalue of the angle-resolved correlation function. The corresponding eigenvector determines the angular dependence of the order parameter.

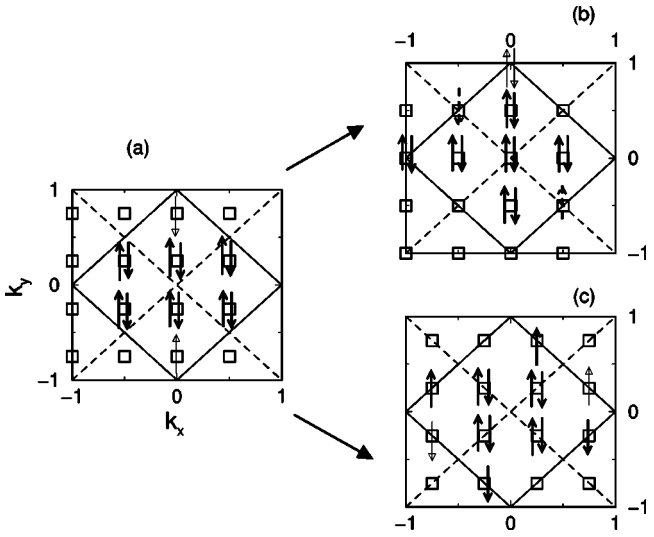

FIG. 2. Reciprocal lattice of the 4×4 cluster assuming (a) mixed boundary conditions, (b) periodic boundary conditions, and (c) antiperiodic boundary conditions. Ground-state configurations corresponding to the fillings $n=0.75$ (thick arrows) and $n=0.875$ (adding the thin arrows to the previous case) are also sketched.

B. Exact diagonalization

This method consists in the exact computation, by recourse to Lanczos algorithm, of the ground-state (g.s.) wave function of the model Hamiltonian (1) on a small cluster. We consider a cluster containing 4×4 lattice sites.

Due to the finite size of the cluster, its reciprocal lattice contains just some few ($N=16$) points. As several instabilities are expected to be competitive in this model, the rough mesh of available $\mathbf{k}$ vectors can produce an important bias and lead to an artificial enhancement of some kind of correlation. The only resort to minimize this drawback is to consider different kinds of boundary conditions, which is equivalent to consider different choices of the 16 $\mathbf{k}$ points. An arbitrary choice of boundary conditions breaks the point group symmetry of the original lattice. Exceptions are the periodic (P) and antiperiodic (AP) boundary conditions, which lead to the mesh indicated in Figs. 2(b) and 2(c), respectively. Mixed (M) boundary conditions (periodic in one direction and antiperiodic in the other) lead to the pattern depicted in Fig. 2(a). The latter breaks some of the symmetries of the C_{4v} group of the original lattice, the corresponding point group being C_{2v}. Typically, these three choices of boundary conditions are the ones leading to the lowest energy. In our study, we compute the g.s. of (1), considering the three abovementioned possibilities within the subspaces corresponding to the different one-dimensional representations of the point group and total $\mathbf{k}=(0,0)$. In the noninteracting system, it is easy to see that closed-shell configurations are those leading to the lowest energy. For some densities of particles this condition is, however, not possible to be fulfilled for any choice of the boundary conditions and the g.s. is degenerate. The interactions normally lift most of the degeneracies. In some cases, it is observed that when the interactions overcome some particular value, a change is produced in the BC leading to the lowest energy. The latter effect is an indication that interactions lead to some qualitative change in the behavior of the g.s. This is, of course, a mere finite size effect but provides a valuable information, since it reflects that the system prefers a change in the population of available $\mathbf{k}$ points in order to take advantage of the interactions and thus lower the energy.

To investigate the superconducting correlations in the g.s. it is useful to study the behavior of the pair correlation function (PCF)

$$P(\mathbf{r})=\frac{1}{N}\sum_i \langle\Psi_0|\Delta_\alpha^\dagger(\mathbf{R}_i+\mathbf{r})\Delta_\alpha(\mathbf{R}_i)|\Psi_0\rangle, \tag{15}$$

where $|\Psi_0\rangle$ is the ground-state wave function while $\Delta_{os}^\dagger(\mathbf{R}_i)=c_{i\uparrow}^\dagger c_{i\downarrow}^\dagger$ for on-site s pairing, $\Delta_\alpha^\dagger(\mathbf{R}_i)=\Sigma_\delta f_\alpha(\delta)[c_{i+\delta\uparrow}^\dagger c_{i\downarrow}^\dagger - c_{i+\delta\downarrow}^\dagger c_{i\uparrow}^\dagger]/\sqrt{8}$, with $f_{es}(\delta)=1$ for extended s pairing, and $f_d(\delta)=1[f_d(\delta)=-1]$ when $\delta=\pm(1,0)[\delta=\pm(0,1)]$ for $d_{x^2-y^2}$ pairing. This function is normalized in such a way that $|\Delta_\alpha^\dagger(i)|\Psi_0\rangle^2=1$. A superconducting state with pairs of a given symmetry is expected to have sizable correlations between pairs far separated by arbitrary large distances. In the case of the 4×4 cluster, the largest available distance is $r=(2,2)$. The PCF between pairs separated by this maximum distance is denoted P_m. As even in the noninteracting limit the PCF can be finite, we interpret an enhancement of the corresponding PCF relative to its value at $U=0$, $J=0$ as an indication of the superconducting instability.

To study the spin-density-wave (SDW) correlations it is useful to compute the spin-spin correlation function

$$S(\mathbf{r})=\frac{1}{N}\sum_i \langle\Psi_0|S^z(\mathbf{R}_i+\mathbf{r})S^z(\mathbf{R}_i)|\Psi_0\rangle, \tag{16}$$

and to analyze the Fourier transform

$$S(\mathbf{k})=\frac{1}{N}\sum_i e^{i\mathbf{k}\cdot\mathbf{R}_i}S(\mathbf{r}), \tag{17}$$

which provides information on the nature of the correlations between spins.

III. RENORMALIZATION-GROUP RESULTS FOR HUBBARD MODEL WITH REPULSIVE AND ATTRACTIVE INTERACTION

In this section we present results for the usual Hubbard model obtained by the RG method described in the previous section. The motivation is twofold. For the case of the $U>0$ model, it was shown in Ref. 41 that self-energy corrections included in the renormalization of $Z(\theta)$ are important to predict the antiferromagnetic instability at half filling in 2D and to recover the correct expression for the jump at the Fermi points in 1D but the behavior of the susceptibilities away from half-filling has not been analyzed so far. On the other hand, for $U<0$ the model is a paradigmatic example of a superconductor and it is, therefore, an important reference point to analyze the behavior of the superconducting correlations. The results shown correspond to a discretization of 32 patches.

When applied to the usual Hubbard model with repulsive interactions ($U>0$), the RG without considering self-energy

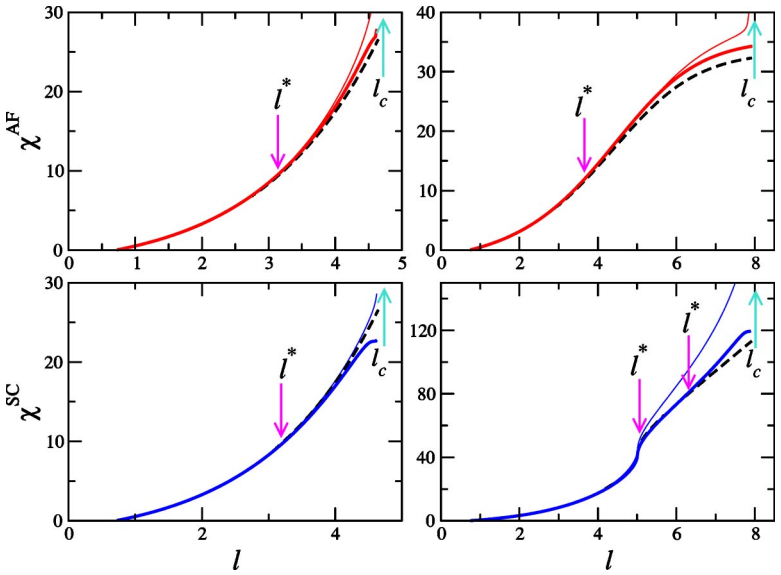

FIG. 3. (Color online) AF (upper panels) and $d_{x^2-y^2}$ SC (lower panels) susceptibilities as functions of the scale l for Hubbard model with $U=1.6t$ and densities determined by $l_\mu=\infty$ (left-hand panels) and $l_\mu=3$ (right-hand panels), corresponding, respectively, to half filling (parquet regime) and high doping (within the BCS regime). Thick and thin lines correspond to results with and without self-energy corrections, respectively. The noninteracting particle-particle and particle-hole susceptibilities are shown in dashed lines. The critical scale l_c as well as the scale l^* at which the susceptibility departs from the behavior of the noninteracting one are indicated with magenta and cyan arrows, respectively.

corrections,[6,8,9] predicts that at some critical scale l_c, the superconducting susceptibility with $d_{x^2-y^2}$ symmetry together with AF susceptibility diverge within the parquet regime ($|\mu|<\Lambda$), even at half filling. This feature is expected to be an artifact of the approximation since for $n=1$ umklapp processes are active and they are expected to drive the system toward an insulating AF state. In Ref. 41 it was shown that, due to the renormalization of the quasiparticle weight, the SC susceptibility is suppressed below its noninteracting value, while the AF susceptibility remains enhanced, although weakly, relative to the noninteracting particle-hole one.

Figure 3 shows the behavior for the different susceptibilities as functions of the scale l, at different densities defined by the chemical potential $\mu=8t\exp(-l_\mu)$. The susceptibilities with and without self-energy corrections are respectively plotted in thin and thick lines. The two left-hand panels correspond to half filling ($l_\mu=\infty$) and summarize the results of Ref. 41. Without self-energy corrections both SC and AF susceptibilities diverge at l_c, AF being dominant. Self-energy effects suppress the divergence, decreasing the SC susceptibility bellow its noninteracting value. The AF susceptibility is also renormalized by self-energy effects but remains larger than the noninteracting one. The scale l^* (see Fig. 3) at which the AF susceptibility begins to depart from the behavior of the noninteracting one is, however, not affected by the self-energy corrections. This kind of behavior extends along the parquet regime, defined by the condition $|\mu|<\Lambda$.

The region at lower densities such that $|\mu|<\Lambda$ is usually called BCS regime because only Cooper channel has logarithmic contributions to the effective interaction. The two right-hand panels of Fig. 3 show how in this regime both AF and SC susceptibilities remain slightly larger than their noninteracting values when self-energy corrections are taken into account.

These results need some discussion. Up to now it was rather widely accepted that the 2D Hubbard model has a $d_{x^2-y^2}$ SC state away from half filling. On the contrary, results on the right-hand panels of Fig. 3 do not convincingly indicate a strong superconducting instability. The SC correlation functions being only weakly enhanced and the scale l^* being strongly renormalized towards high values when self-energy effects are taken into account (see right-hand lower panel of Fig. 3). This indicates that the energy $\Lambda^*=8t\exp(-l^*)$ at which superconducting correlations begin to manifest themselves decreases when self-energy effects are considered. At Λ_c there is a creation of bound states because the four-point vertex (5) has poles. These bound states are the gapless modes that destroy the one-particle coherence via self-energy corrections and the result is that the phase transition is suppressed, probably to some finite lower energy.

To justify the above interpretation we calculated for comparison the RG flow of the attractive Hubbard model, for which the instabilities are better known. The $U<0$ model is a paradigmatic example of *s*-wave-type superconductor and its phase diagram has been investigated in detail by mean-field and numerical techniques. Unlike the repulsive counterpart, predictions by different methods agree about the main instabilities expected in its phase diagram.[43,44] At weak coupling, the explicit local negative interaction leads to BCS-like superconductivity away from half filling. For $n=1$, local CDW is believed to be degenerate with *s*-wave superconductivity in the g.s.[43] In 1D, such degeneracy is exact due to symmetry reasons. This is because the repulsive model has dominant AF correlations with a power law decay. Since no breaking of the SU(2) symmetry is possible, the behavior of the correlations in any of the spacial direction must behave in the same way. On another hand, there is an exact transformation $c^\dagger_{i\uparrow}\to(-1)^i c_{i\uparrow}$, $c^\dagger_{i\downarrow}\to c^\dagger_{i\downarrow}$, which maps the repulsive model into the attractive one, while maps the degenerate z and x,y components of the dominant SDW correlations of the $U>0$ model to the CDW and superconducting ones, respectively, of the $U<0$ counterpart. The above reasoning can also be extended to the 2D case provided that no symmetry breaking in the ground state of the $U>0$ model takes place. Results obtained with RG for the attractive model in 2D shown in Fig 4 are in very good agreement with the description provided by numerical methods.[43,44] At half filling ($l_\mu=\infty$, see left-hand panels of Fig. 4), the most remarkable feature is the degeneracy observed between CDW and SC

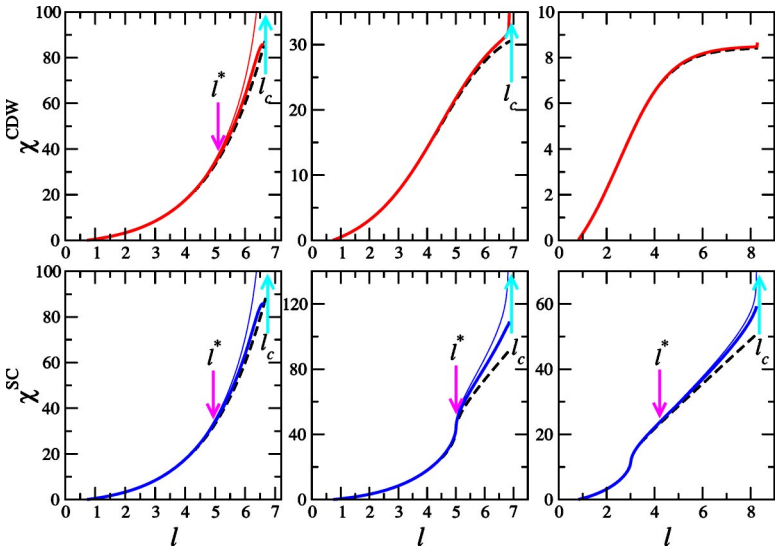

FIG. 4. (Color online) CDW (upper panels) and *s*-wave SC (lower panels) susceptibilities as functions of the scale l for $U=-0.8t$ and densities determined by $l_\mu=\infty$, 5, 3, corresponding to half filling and two densities within the BCS regime (from left to right). Other details are the same as in Fig. 3.

susceptibility with local *s*-wave symmetry, which remain slightly larger than the noninteracting one when self-energy corrections are considered. This should be rather expected since the present method provides a description of the normal state and only the onset of the instability towards the symmetry broken state is captured. Below half filling ($l_\mu=5$, 3, see middle and right-hand panels of Fig 4), CDW susceptibility becomes weaker, approximately equal to the noninteracting one, while the superconducting susceptibility becomes more enhanced. Self-energy effects suppress the divergence of the different instabilities but do not renormalize the scale l^*.

Below half filling, the *s*-wave type SC susceptibility is clearly larger than the noninteracting particle-particle one. As expected, the CDW remains non renormalized. Compared to the repulsive Hubbard model (Fig. 3), the enhancement of SC correlations is more convincing and in the present case we can indeed assign the divergence at l_c to the onset of the *s*-wave superconductivity. Altogether, the attractive Hubbard model away from half filling shows strong tendencies towards the *s*-wave superconductivity even when the self-energy corrections are taken into account. This is in contrast to the repulsive case where the self-energy effects have a more pronounced effect against the $d_{x^2-y^2}$ superconductivity. The reason for this behavior is rather simple: the *s*-wave superconductivity in the attractive Hubbard model is an effect of first order in U, while the self-energy corrections are of second order. As long as the coupling is weak the BCS-like instability is a good approximation. Formally this means that the mean-field and the Kosterlitz-Thouless transitions are close to one another. In the case of the repulsive interaction the $d_{x^2-y^2}$ superconductivity and the self-energy corrections are both of second order in U, so that by decreasing U one cannot promote only superconductivity and make the fluctuations subdominant.

IV. RENORMALIZATION-GROUP RESULTS FOR THE *t-J-U* MODEL

We present results for the relevant susceptibilities in the *t-J-U* model in Fig. 5. The left-hand panels correspond to half filling and the behavior is similar to that of the Hubbard case. Namely, SC susceptibility with $d_{x^2-y^2}$ symmetry evolves to values below of the noninteracting one, while AF susceptibility remains higher than its noninteracting value, indicating that at $n=1$, the system flows towards an AF insulating state. Upon doping the $d_{x^2-y^2}$ superconductivity gets progressively stronger and becomes the dominant instability at about the crossover line $\Lambda=\mu$, just as in the Hubbard model. The right-hand panels show a typical flow of the susceptibility in the BCS regime ($\Lambda<\mu$) where the dominant correlations are of superconductivity type.

The above picture shares some features with the behavior observed in the Hubbard model, discussed in the previous section. Important issues to highlight are as follows. (i) At half filling the behavior of the relevant susceptibilities is very similar to that of the repulsive Hubbard model. However, the scale l_c at which the onset of the AF instability takes place as well as the scale l^* are smaller than for the $J=0$ case. The susceptibility is also significantly larger than the noninteracting one, even when self-energy corrections are included in the RG procedure. These features indicate that J contributes to increase the AF correlations and the Néel temperature. (ii) At higher dopings, within the BCS regime, AF susceptibility coincides with the noninteracting one while SC correlations become significantly enhanced. This is in contrast to the behavior of the repulsive model (see Fig. 3) where SC correlations are only weakly enhanced. Instead, the behavior on the right panels of Fig. 5 resembles the one of the attractive Hubbard model, if we associate $d_{x^2-y^2}$ SC and AF susceptibilities in Fig. 5, respectively, to *s*-wave SC and CDW susceptibilities on middle and right panels of Fig. 4. Also note that, as in the attractive model, the scale l^* remains unaffected by self-energy effects. In addition, the scale l_c at which the onset of the superconducting instability is observed is small in the *t-J-U* model, implying a high critical temperature. We have carried out a similar analysis for other values of the parameters J and U and found that the symmetry of the dominant superconducting correlations is always $d_{x^2-y^2}$. We have verified the reliability of these results upon increasing number of patches up to 64 patches. The reason

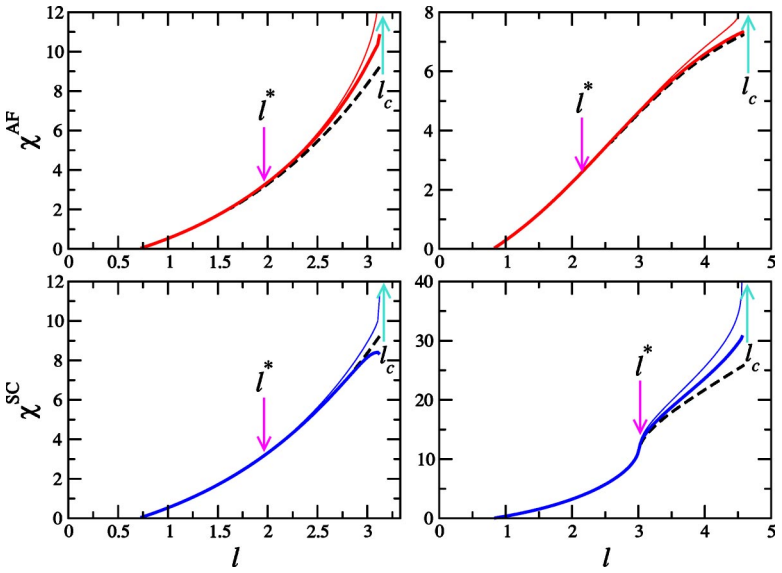

FIG. 5. (Color online) AF (upper panels) and $d_{x^2-y^2}$ SC (lower panels) susceptibilities as functions of the scale l for Hubbard model with $U=J=1.6t$ and densities determined by $l_\mu=\infty$ (left-hand panels) and $l_\mu=3$ (right-hand panels), corresponding, respectively, to half filling (parquet regime) and high doping (within the BCS regime). Other details are the same as in Fig. 3.

for the robustness of the SC correlations is in the fact that the J interaction has an attractive $d_{x^2-y^2}$ SC component, so that superconductivity exists already at first order of U_l while the fluctuations are only subdominant, just as in the attractive Hubbard case.

In order to have a more quantitative representation of the role played by both interactions we present the phase diagram in Fig. 6. The "critical temperature" plotted in the figure is defined as $T_c \sim \Lambda_c$, where $\Lambda_c = 8t \exp(-l_c)$. Results for the repulsive Hubbard model are also shown for comparison. By comparing the plots for $J=0$, $U=1.6t$ and $J=1.6t$, $U=0$ in the left panel and for $J=0$, $U=1.6t$ and $J=0.4t$, $U=1.6t$ in the right panel (the arrows are drawn to ease the reading), it is clear that J is a remarkably efficient mechanism to drive AF close to half filling and $d_{x^2-y^2}$ superconductivity in the doped system. Another important feature is that at fixed J, the effect of U is to increase the "critical temperature." This means that the two interactions are not competitive but, instead, cooperate to increase the strength of antiferromagnetic and superconducting correlations.

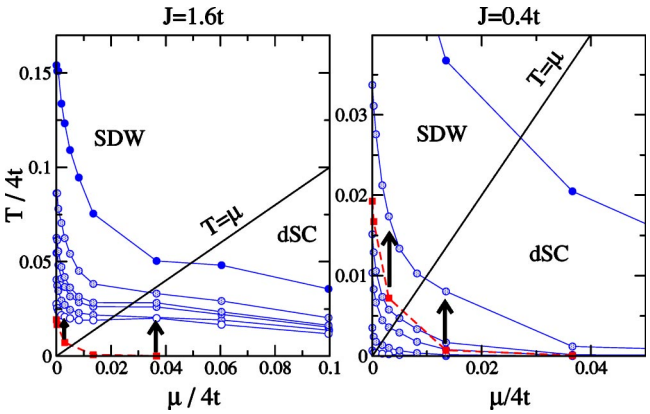

FIG. 6. (Color online) Phase diagram showing combined action of U and J interactions. The "critical temperature" is defined as $T_c \sim \Lambda_c = 8t \exp(-l_c)$ (see text). Left and right panels correspond to $J=1.6t$ and $J=0.4t$, respectively. Plots in blue circles correspond to $U=0,\ 0.4t, 0.8t, t, 1.6t, 3.2t$. The ones corresponding to the lowest and highest U are drawn in open and dark filled symbols, respectively. The plot in red squares corresponds to the usual Hubbard model ($J=0$ and $U=1.6t$). The line $T=\mu$ separates the regions where the SDW and $d_{x^2-y^2}$ superconducting (dSC) instabilities are the dominant ones.

V. EXACT-DIAGONALIZATION RESULTS FOR THE *t-J-U* MODEL IN THE 4×4 CLUSTER

The results of the previous section suggest that the combined effect of the interactions J and U drives superconductivity with $d_{x^2-y^2}$ symmetry in the doped system, leading to a significant enhancement of the superconducting correlations. As in the case of the pure Hubbard model numerical methods fail to detect the tendency towards $d_{x^2-y^2}$ superconductivity, it is interesting to analyze the case of finite J.

We show below results obtained by following the strategy explained in Sec. II. We computed the exact g.s. energy and wave function in a 4×4 cluster and calculated the correlation functions between pairs with local and extended s-wave and $d_{x^2-y^2}$ symmetries. We focused our attention on the study of three different fillings ($n=0.625$, 0.75, 0.875), corresponding to $N=10$, 12, 14 particles in the cluster.

Let us begin with the analysis of the boundary conditions leading to the lowest energy. For the case $n=0.625$, the g.s. is obtained for PBC. In the noninteracting limit, it corresponds to a closed-shell configuration and for all the explored values of the interactions, it lies in the subspace associated to the representation of the point group with s-wave-like character. The $\mathbf{k}$ points lying on the Fermi surface of the noninteracting system are $(\pi/2, 0)$ and the symmetry related points. For these points, the structure factors $f_{es}(\mathbf{k}) = \cos(k_x) + \cos(k_y)$ and $f_d(\mathbf{k}) = \cos(k_x) - \cos(k_y)$, corresponding to BCS gaps with extended s and $d_{x^2-y^2}$-wave symmetries have exactly the same strength $|f_d| = |f_{es}| = 1$.

For fillings $n=0.75$ and $n=0.875$, the lowest energy in the noninteracting case is achieved by considering MBC. In this limit, the only ingredient playing a role in the energetic balance is the kinetic energy gain. As interactions are switched

TABLE I. Ground-state energy per site for the 4×4 cluster with particle density $n=0.75$. Stars indicate states with APBC and the representation of the point group that transforms similar to an *s* wave. Otherwise the states correspond to MBC.

U	$J=0$	$J=0.25$	$J=0.5$	$J=0.75$	$J=1$	$J=1.5$	$J=1.75$	$J=2$
0	−1.5607	−1.5940	−1.6298	−1.6681	−1.7092	−1.8006	−1.8514	−1.9057
2	−1.3233	−1.3651	−1.4101	−1.4584	−1.5100	−1.6239	−1.6864	−1.7526
4	−1.1607	−1.2094	−1.2616	−1.3176	−1.3772	−1.5075	−1.5803*	−1.6619*
6	−1.0516	−1.1045	−1.1615	−1.2225	−1.2874	−1.4291*	−1.5125*	−1.5975*
8	−0.9774	−1.0326	−1.0924	−1.1565	−1.2247	−1.3773*	−1.4630*	−1.5503*
10	−0.9255	−0.9818	−1.0430	−1.1089	−1.1792	−1.3385*	−1.4258*	−1.5145*
12	−0.8878	−0.9445	−1.0065	−1.0735	−1.1451	−1.3087*	−1.3969*	−1.4867*
14	−0.8596	−0.9162	−0.9786	−1.0463	−1.1187	−1.2852*	−1.3741*	−1.4645*
16	−0.8377	−0.8942	−0.9567	−1.0247	−1.0977	−1.2662*	−1.3556*	−1.4465*
18	−0.8204	−0.8765	−0.9391	−1.0073	−1.0807	−1.2505*	−1.3403*	−1.4315*
20	−0.8063	−0.8621	−0.9246	−0.9929	−1.0666	−1.2375*	−1.3275*	−1.4189*

on, the g.s. corresponds to APBC for sufficiently large J and U. This indicates that the **k** points tuned by APBC are able to take advantage of some effect of the interactions, compensating the loss of kinetic energy. For the latter boundary conditions, the Fermi points of the noninteracting system lie on the lines of nodes of f_{es}. Therefore, it is likely that the most favored instability by such a change of population in the **k** space is $d_{x^2-y^2}$-wave superconductivity. Some values of the GS energy per site are shown in Tables I and II.

It is interesting to note that, for the density $n=0.75$, the g.s. belongs to the representation of the point symmetry group with *s*-wave-like character within the region where the g.s. corresponds to APBC. Instead, for $n=0.875$ and also within the region of parameters where the g.s. corresponds to APBC, the character of the point-group representation is $d_{x^2-y^2}$-wave-like. Since in the present cluster $n=0.875$, differs from $n=0.75$ in two particles, this change of representation is consistent with the idea that a pair of particles with $d_{x^2-y^2}$-wave symmetry was added to a many-particle background with total *s*-wave symmetry. We actually speculate that such a background is also made up of paired particles.

The behavior of P_m, the pair correlation function (15) corresponding to pairs separated by the maximum possible distance of the cluster, for a particle density $n=0.625$ is shown in Fig. 7. The correlation function corresponding to local pairs with *s*-wave symmetry is much weaker and is not shown. The corresponding values for the noninteracting system are indicated in dot-dashed lines to ease the comparison. In the latter limit, correlations of pairs with $d_{x^2-y^2}$ symmetry remain weaker than those of the noninteracting case while *s*-wave ones are slightly enhanced for small enough U. The effect of J is to produce a weak enhancement of P_m within the two symmetry channels in comparison to the pure Hubbard case. In particular, $d_{x^2-y^2}$ ones become stronger than those of the noninteracting case for small enough U.

The pairing function P_m for the density $n=0.75$ is shown in Fig. 8. We have analyzed the behavior using the two boundary conditions leading to the lowest energy. In the case of APBC shown in the upper panel of Fig. 8, only the correlation of pairs with $d_{x^2-y^2}$ symmetry is shown, since those

TABLE II. Ground state energy per site for the 4×4 cluster with particle density $n=0.875$. Stars indicate states with APBC and the representation of the point group that transforms similar to a $d_{x^2-y^2}$ wave. Otherwise the states correspond to MBC.

U	$J=0$	$J=0.25$	$J=0.5$	$J=0.75$	$J=1$
0	−1.6339	−1.6690	−1.7074	−1.7496	−1.7967
2	−1.2936	−1.3404	−1.3937	−1.4547	−1.5240
4	−1.0473	−1.1091	−1.1812	−1.2625	−1.3514
6	−0.8805	−0.9571	−1.0445	−1.1394	−1.2404*
8	−0.7712	−0.8580	−0.9540	−1.0566	−1.1685*
10	−0.6978	−0.7897	−0.8908	−0.9991*	−1.1154*
12	−0.6460	−0.7406	−0.8446	−0.9568*	−1.0751*
14	−0.6079	−0.7037	−0.8095	−0.9239*	−1.0437*
16	−0.5788	−0.6752	−0.7819	−0.8979*	−1.0186*
18	−0.5560	−0.6524	−0.7598	−0.8768*	−0.9982*
20	−0.5376	−0.6338	−0.7417	−0.8594*	−0.9812*

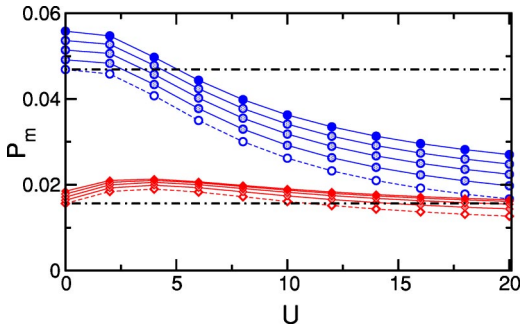

FIG. 7. (Color online) Pair correlation function at the maximum distance P_m of the cluster for a density of particles $n=0.625$. Blue circles correspond to pairs with $d_{x^2-y^2}$ and red diamonds to extended *s* symmetry. Different plots correspond to $J=0$, 0.25, 0.5, 0.75, 1. Open and filled dark symbols correspond to the lowest and highest value of *J*, respectively. The dotted-dashed line indicates the value of P_m in the noninteracting limit.

with local-*s* and extended-*s* waves are negligibly small in comparison. In the case of MBC shown in the lower panel, correlations in both, extended *s*-wave and $d_{x^2-y^2}$-symmetry channels are only slightly enhanced for some values of *J* and suppressed for others. Instead, for APBC, a clear enhancement of the correlations of pairs with $d_{x^2-y^2}$ is observed as *J* is switched on. Note that, in contrast to the case $J=0$, the correlation function P_m lies above the line indicating the magnitude of P_m in the noninteracting case.

Similar remarks apply to the behavior of P_m at the density $n=0.875$, shown in Fig. 9. The enhancement of $d_{x^2-y^2}$ pairing correlations for the case of APBC is related to the fact that the available **k** vectors mainly populated in the ground state contribute with a sizable structure factor to a pairing interaction at the Fermi surface with $d_{x^2-y^2}$ symmetry.

If, for the latter densities, we plot the pair correlation function in the GS corresponding to the optimal boundary condition (i.e., that leading to the lowest energy), we obtain

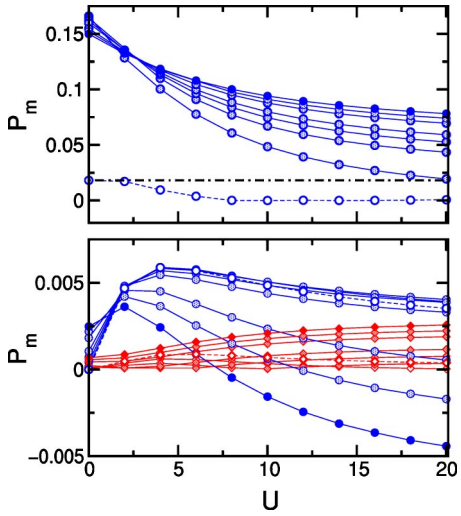

FIG. 8. (Color online) Pair correlation function at the maximum distance of the 4×4 cluster P_m for a density of particles $n=0.75$. Different plots correspond to $J=0$, 0.25, 0.5, 0.75, 1, 1.5, 1.75, 2. Upper and lower panels correspond to APB and MBC, respectively. Other details are as in Fig. 7.

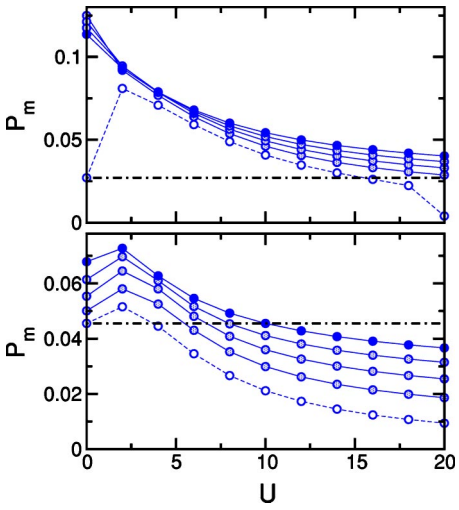

FIG. 9. (Color online) Pair correlation function at the maximum distance of the 4×4 cluster P_m for a density of particles $n=0.875$. Other details are as in Fig. 8.

the picture shown in Fig. 10. In good agreement with the analysis done in the discussion about the behavior of the g.s. energy, we see that the change in the boundary condition leading to the lowest energy, is accompanied with an enhancement of the $d_{x^2-y^2}$-wave pairing correlation function. The pairing correlation functions with extended *s* symmetry are, instead, vanishing small within all the range of parameters. This could be an unfortunate consequence of the small size of the cluster and to the fact that the most populated **k** points when the boundary conditions change, lie on the lines of nodes of the structure factor f_{es}. However, this behavior is in agreement with the results predicted by RG.

To finalize, we present some results on the behavior of spin-spin correlation functions. Figures 11 and 12 show some typical plots corresponding to the g.s. in the cluster with

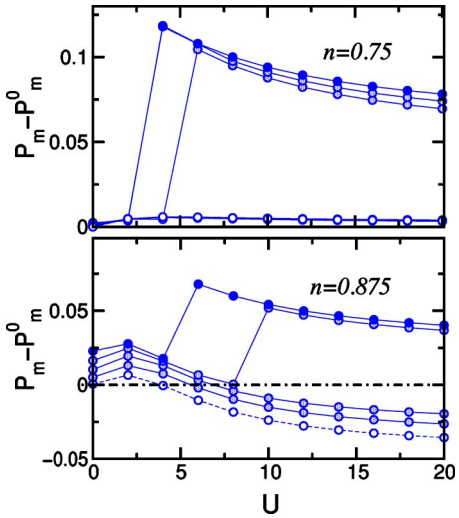

FIG. 10. (Color online) Pair correlation function at the maximum distance of the 4×4 cluster P_m for pairs with $d_{x^2-y^2}$ symmetry corresponding to the optimal boundary conditions for the ground state. Upper and lower panels correspond to densities of particles $n=0.75$ and $n=0.875$, respectively. Other details are as in Figs. 7 and 8.

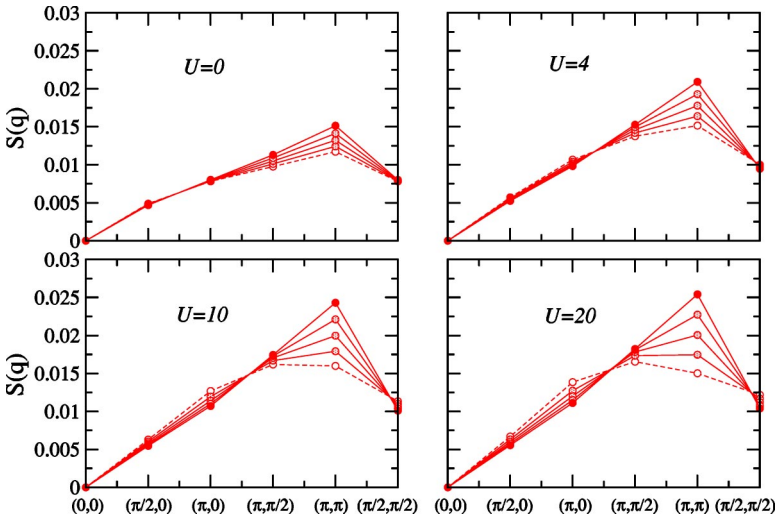

FIG. 11. (Color online) Fourier transform of the spin-spin correlation function for $n=0.75$ and MBC. Different panels correspond to different U. Open and filled dark symbols correspond to $J=0$ and $J=1$, respectively. Other plots correspond to intermediate equally spaced values of J.

MBC. In the case of Fig. 11 the latter boundary condition corresponds to the one leading to the lowest energy within the range of parameters shown. In Fig. 12 this is not always the case but we found that there are only slight quantitative differences between the results of the figure and the corresponding ones with APBC. The important feature to note is that the effect of J is to increase the peak of $S(\pi,\pi)$. By comparing the height of the latter peak for the two densities it is clear that AF correlations increase as the system approaches to half filling. For $n=0.75$, $S(\mathbf{k})$ shows a wide structure for the usual Hubbard model, and for large U the peak is placed at incommensurate positions $\mathbf{k}\neq(\pi,\pi)$ (see lower panels of Fig. 11). Remarkably, the effect of J is to shift these peaks to the AF vectors. All these features are consistent with the idea that J drives an enhancement of AF correlations relative to the usual Hubbard case. The small size of the cluster does not allows us to have an estimate of the AF correlation length. It can be, however, noted that for the lower density (see Fig. 11) $S(\mathbf{k})$ spreads out on a wide range of $\mathbf{k}$ vectors surrounding (π,π), consistent with a picture of short-range AF correlations. Instead, for lower doping, the structure evolves to a sharper peak around (π,π) suggesting larger coherence lengths. It is also interesting to note that the increment of AF correlations (from $n=0.75$ to $n=0.875$) is accompanied by a decrease of the pairing correlations (see Fig. 6), in agreement with the RG results from the previous section.

VI. SUMMARY AND CONCLUSIONS

The main result of the present study is that the cooperative effect between the nearest-neighbor exchange interaction J and the on-site Coulomb repulsion U increases in a larger than simply additive way the antiferromagnetic and $d_{x^2-y^2}$ superconducting tendencies in 2D. For our analysis we used the angle resolved renormalization group including self-energy corrections and the exact diagonalization methods.

We have first considered the repulsive and the attractive Hubbard models and we have calculated the self-energy-dressed dominant correlation functions at half-filling and at finite doping. In the repulsive ($U>0$) case self-energy effects reduce radically all two-particle correlations and destroy their divergences near the critical scale. At half filling the SC correlation function is below its $U=0$ value, while the AF one remains stronger than its value for $U=0$, but loses the divergence. This behavior, discussed in Ref. 41, is a signature of the Mott localization tendencies with simultaneous build up of short-ranged AF correlations. At finite doping, surprisingly and contrary to previous predictions made by the RG theory without self-energy corrections (Ref. 6), the superconducting instabilities are strongly reduced by self-energy corrections even deeply in the BCS regime, i.e., when the Fermi surface is badly nested and umklapps are irrelevant. In the case of the attractive interaction ($U<0$) our RG results are in complete agreement with previous studies.[43,44] At half filling the s-wave superconductivity and the charge density wave correlations are degenerate. The flow of the two correlation functions looks similar to the one of the AF correlation function for repulsive Hubbard model at half filling. Just as in the repulsive case, the self-energy effect regularizes the flow of correlation functions near Λ_c at half filling and no phase transition occurs at this scale. The effective action of the regime below Λ_c was discussed by Schulz.[45] Contrary to the half-filled case, at finite doping the attractive Hubbard model shows a convincing onset of the superconductivity. In comparison to the repulsive case where $d_{x^2-y^2}$ SC susceptibility is only weakly enhanced, in the attractive case the s-wave SC correlations at Λ_c are not destroyed by the self-energy, while CDW susceptibility remains stuck to its $U=0$ value. At this point some general remarks are in order. We have seen that there are fundamental differences between RG flows of the repulsive and of the attractive Hubbard models. The fluctuations in the repulsive model are much stronger and probably fatal for superconductivity. They tend not only to decrease the magnitude of the SC susceptibility but also to decrease the energy $\Lambda^*=8t\exp(-l^*)$ at which it begins to depart from the behavior of the noninteracting one. Our present study is unable to say if the superconductivity is stabilized or not at some energy lower than Λ_c. However, the absence of all divergences indicates that the scenarios with preformed pairs of AF and SC type are relevant even in the weak coupling limit. These RG results

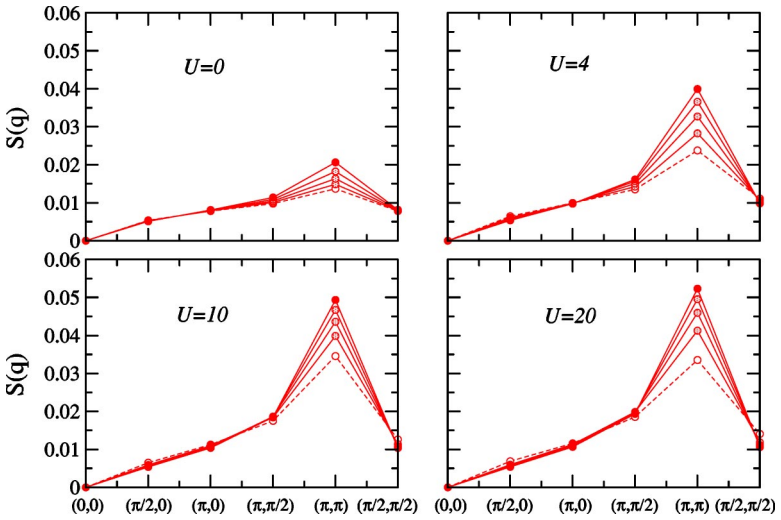

FIG. 12. (Color online) The same as Fig. 11 for $n=0.875$.

agree with the ED analysis for the intermediate-to-strong couplings, where no superconductivity was detected. The situation is fundamentally different in the attractive Hubbard model, where the superconducting instability is robust upon self-energy corrections. This is the RG version of the well known fact that the incoherent preformed pairs can live only at intermediate-to-strong interaction.[46]

The study of the two Hubbard models was a necessary introduction to the RG analysis of the *t-J-U* model. The question that we answer is if the superconductivity of the *t-J-U* model is enhanced or reduced with respect to the simple cases $J=0$ and $U=0$. The answer is that J and U cooperate to (a) increase the critical cutoff and (b) keeping the renormalized susceptibility enhanced relative to the noninteracting one. We also found that the latter effect is observed not only on the superconducting side of the phase diagram but also on the antiferromagnetic one. We thus have an evidence for the *U-J* synergy effect. The phase diagram on Fig. 6 shows in particular the cases ($U=1.6t$, $J=0$), ($U=0$, $J=1.6t$), and ($U=1.6t$, $J=1.6t$). The critical temperature of the third case is much higher than for the first two, while the onset of $d_{x^2-y^2}$ SC remains convincingly large in the flow of the correlation function.

Exact-diagonalization results support the above picture. In fact, for large enough J and U, we find below half filling a clear enhancement of the SC correlations with $d_{x^2-y^2}$[21] symmetry which is accompanied by a change in the type of boundary conditions leading to the lowest energy. This behavior is consistent with the idea that the large Coulomb repulsion spreads out the Fermi surface towards sectors of the Brillouin zone where the interaction J has the largest amplitude in the BCS channel with $d_{x^2-y^2}$ symmetry. In such a way, we can think that particles are pushed to a region of the phase space, where the attractive interaction is most efficient to organize them into pairs. Similar arguments can be proposed to explain the enhancement of AF correlations at half filling since the J interaction has components along AF and SC channels. In particular, in Ref. 41 it has been found that the angle-resolved quasiparticle weight $Z(\theta)$ renormalizes in such a way that it displays a maximum in regions of the Fermi surface that are separated by the magnetic vector $Q=(\pi,\pi)$. We have not found strong differences between the behavior of $Z(\theta)$ in the usual Hubbard model and the *t-J-U* one neither at half filling nor for finite doping. Therefore, the most likely scenario at half filling is that the larger population of convenient regions of the k space become available to be exploited by the component of the J interaction along the AF channel.

We have not found any indication of bond-order-like instability. This is in disagreement with some mean-field predictions[26] but in full agreement with other RG studies on van-Hove fillings of the *t-t′-J-U* models.[40] Our conclusion regarding the combined *J-U* mechanism to drive large superconducting correlations is also in agreement with previous investigations based on Fermi liquid arguments and quantum Monte Carlo simulations.[39] Within the repulsive Hubbard model, we obtained by renormalization group that the self-energy corrections are fatal for superconductivity and by exact diagonalization that the superconductivity is unlikely. This result is important because it reconciles the N-patch RG with exact diagonalization *and* with a number of other approaches. Our results show that while the $d_{x^2-y^2}$ pairing exists in the Hubbard model (because vertex indeed diverges), the onset of macroscopic superconductivity is suppressed. This result is in agreement with the very recent findings by Plekhanov and co-workers.[47]

All above remarks indicate that the J interaction is vital for the superconductivity while the U interaction increases considerably the tendency towards pair formation. They also suggest that minimal microscopic models supporting recent phenomenological proposals for colossal effects in the phase diagram of the high-T_c compounds[1] may be based on these two interactions. In fact, our results indicate that the interaction J provides a kick to the potential or weak antiferromagnetic and superconducting tendencies of the Hubbard model, that triggers a gigantic response in the system. This picture resembles the behavior of manganites where colossal magnetoresistance effects take place in response to external magnetic fields and this analogy is behind the proposal of Ref. 1. The appropriate microscopic approach should be based on a recently developed N-patch renormalization group theory for disordered and interacting imperfectly nested system.[48] On

the other hand, as discussed in our introductory section, derivations starting from the three band model for the cuprates also support the idea that the *t-J-U* model is a good candidate for a minimal one-band Hamiltonian for these materials.

ACKNOWLEDGMENTS

We thank Elbio Dagotto for encouraging remarks. LA thanks Professor Fulde for his kind hospitality at the Max-Planck Institut für Physik komplexer Systeme, Dresden, where a good part of this work has been carried out, as well as the support of the Alexander von Humboldt Stiftung, CONICET, Argentina, Laboratoire de Physique Théorique et Hautes Energies is CNRS UMR 7589 at Universities Paris VI Pierre et Marie Curie and Paris VII Denis Diderot. Support from the Grant No. PICT 03-11609 of AIC of Argentina and from MCyT of Spain through the Ramón y Cajal program is also acknowledged.

*Present address: Instituto de Biocomputación y Física de Sistemas Complejos, Zaragoza, Spain.

[1] G. Alvarez, M. Mayr, A. Moreo, and E. Dagotto, cond-mat/0401474 (unpublished).
[2] N. E. Bickers, D. J. Scalapino and S. R. White, Phys. Rev. Lett. **62**, 961 (1989).
[3] T. Dahm and L. Tewordt, Phys. Rev. Lett. **74**, 793 (1995).
[4] J. Schmalian, Phys. Rev. Lett. **81**, 4232 (1998).
[5] J. González, F. Guinea, and M. A. H. Vozmediano Phys. Rev. Lett. **79**, 3514 (1997).
[6] D. Zanchi ad H. J. Schulz, Phys. Rev. B **61**, 13 609 (2000).
[7] D. Zanchi ad H. J. Schulz, Phys. Rev. B **54**, 9509 (1996).
[8] C. J. Halboth and W. Metzner, Phys. Rev. B **61**, 7364 (2000).
[9] C. Honerkamp, M. Salmhofer, N. Furukawa, and T. M. Rice, Phys. Rev. B **63**, 035109 (2001).
[10] J. Mráz and R. Hlubina, Phys. Rev. B **67**, 174518 (2003).
[11] A. Moreo, Phys. Rev. B **45**, 5059 (1992).
[12] F. F. Assaad, W. Hanke, and D. J. Scalapino, Phys. Rev. Lett. **71** 1915 (1993)
[13] A. F. Veilleux, A. Daré, L. Chen, Y. M. Vilk, and A.-M. S. Tremblay, Phys. Rev. B **52**, 16 255 (1995).
[14] S. Zhang, J. Carlson, and J. E. Gubernatis, Phys. Rev. Lett. **78**, 4486 (1997).
[15] G. Kotliar, Phys. Rev. B **37**, 3664 (1988).
[16] E. Dagotto and J. Riera, Phys. Rev. Lett. **70**, 682 (1993).
[17] E. Dagoto, Rev. Mod. Phys. **66**, 763 (1994).
[18] S. Sorella, G. B. Martins, F. Becca, C. Gazza, L. Capriotti, A. Parola, and E. Dagotto, Phys. Rev. Lett. **88**, 117002 (2002).
[19] M. E. Simon, M. Baliña, and A. A. Aligia, Physica C **206**, 297 (1993); M. E. Simon, A. A. Aligia, and E. Gagliano, Phys. Rev. B **56**, 5637 (1997).
[20] L. Arrachea and A. A. Aligia, Phys. Rev. Lett. **73**, 2240 (1994).
[21] L. Arrachea, A. A. Aligia, and E. Gagliano, Phys. Rev. Lett. **76**, 4396 (1996).
[22] L. Arrachea, E. Gagliano, and A. A. Aligia, Phys. Rev. B **55**, 1173 (1997).
[23] L. Arrachea and A. A. Aligia, Phys. Rev. B **59**, 1333 (1999); **61**, 9686 (2000).
[24] A. A. Aligia and L. Arrachea, Phys. Rev. B **60**, 15 332 (1999).
[25] The effective model is actually more general, containing in addition a nearest-neighbor Coulomb interaction *V*, a hopping of local pairs *X*, and a bond-charge interaction Δ. However, the only interaction driving superconductivity with $d_{x^2-y^2}$ symmetry at mean-field level is *J* and for this reason this is the only one we keep in the present work.
[26] Sudip Chakravarty, R. B. Laughlin, Dirk K. Morr, and Chetan Nayak, Phys. Rev. B **63**, 094503 (2001).
[27] J. E. Hirsch, Phys. Rev. B **65**, 184502 (2002); **67**, 035103 (2003).
[28] F. Guinea, Eur. Phys. J. B **36**, 519 (2003).
[29] I. Martin, G. Ortiz, A. V. Balatsky, and A. R. Bishop, Europhys. Lett. **56**, 849 (2001).
[30] J. Japaridze and A. Kampf, Phys. Rev. B **59**, 12 822 (1999); J. Dai, X. Feng, T. Xiang, and Yue Yu, *ibid.* **70**, 064518 (2004).
[31] J. Vidal and B. Douçot, Phys. Rev. B **65**, 045102 (2002).
[32] F. Dolcini and A. Montorsi, Phys. Rev. B **65**, 155105 (2002); F. Dolcini and A. Montorsi, *ibid.* **66**, 075112 (2002).
[33] M. Tsuchiizu and A. Furusaki, Phys. Rev. B **69**, 035103 (2004).
[34] C. Bourbonnais and D. Jérome, Science **281**, 1155 (1998).
[35] D. K. Campbell, T. A. DeGrand, and S. Mazumdar, Phys. Rev. Lett. **52**, 1717 (1994).
[36] J. Voit, Rep. Prog. Phys. **58**, 977 (1995).
[37] J. Voit, Phys. Rev. B **45**, 4027 (1992).
[38] S. Daul, D. J. Scalapino, and S. R. White, Phys. Rev. Lett. **84**, 4188 (2000).
[39] E. Plekhanov, S. Sorella, and M. Fabrizio, Phys. Rev. Lett. **90**, 187004 (2003).
[40] A. P. Kampf and A. A. Katanin, Phys. Rev. B **67**, 125104 (2003).
[41] D. Zanchi, Europhys. Lett. **55**, 376 (2001).
[42] F. Vistulo de Abreu and B. Douçot, Phys. Rev. Lett. **86** 2866 (2001).
[43] A. Moreo and D. J. Scalapino, Phys. Rev. Lett. **66**, 946 (1991).
[44] N. Trivedi and M. Randeria, Phys. Rev. Lett. **75**, 312 (1995).
[45] H. J. Schulz, cond-mat/9402103 (unpublished).
[46] F. Pistolesi and G. C. Strinati, Phys. Rev. B **53**, 15 168 (1996).
[47] E. Plekhanov, F. Becca, and S. Sorella, cond-mat/0404206 (unpublished).
[48] S. Dusuel and D. Zanchi, Phys. Rev. Lett. **93**, 206401 (2004).